Differential Quasi-Yagi Antenna and Array

ZHU Zhihao[1], ZHANG Yueping[2]
(1. Key Laboratory of Ministry of Education of Design and Electromagnetic Compatibility of High-Speed Electronic Systems, Shanghai Jiao Tong University, Shanghai 200240, China;
2. Nanyang Technological University, Singapore 639798, Singapore)

DOI: 10.12142/ZTECOM.202303006
https://link.cnki.net/urlid/34.1294.TN.20230804.1848.002, published online August 7, 2023
Manuscript received: 2023-03-11

Abstract: A novel differential quasi-Yagi antenna is first presented and compared with a normal single-ended counterpart. The simulated and measured results show that the differential quasi-Yagi antenna outperforms the conventional single-ended one. The differential quasi-Yagi antenna is then used as an element for linear arrays. A study of the coupling mechanism between the two differential and the two single-ended quasi-Yagi antennas is conducted, which reveals that the TE_0 mode is the dominant mode, and the driver is the decisive part to account for the mutual coupling. Next, the effects of four decoupling structures are respectively evaluated between the two differential quasi-Yagi antennas. Finally, the arrays with simple but effective decoupling structures are fabricated and measured. The measured results demonstrate that the simple slit or air-hole decoupling structure can reduce the coupling level from −18 dB to −25 dB and meanwhile maintain the impedance matching and radiation patterns of the array over the broad bandwidth. The differential quasi-Yagi antenna should be a promising antenna candidate for many applications.

Keywords: differential quasi-Yagi antenna and array; mutual coupling; surface wave

Citation (Format 1): ZHU Z H, ZHANG Y P. Differential quasi-Yagi antenna and array [J]. ZTE Communications, 2023, 21(3): 37 – 44. DOI: 10.12142/ZTECOM.202303006
Citation (Format 2): Z. H. Zhu and Y. P. Zhang, "Differential quasi-Yagi antenna and array," *ZTE Communications*, vol. 21, no. 3, pp. 37 – 44, Sept. 2023. doi: 10.12142/ZTECOM.202303006.

1 Introduction

With the trend toward the system-on-chip (SoC) and system-in-package (SiP) solutions of radio and radar transceivers, differential antennas are getting popular for their advantages such as low cross-polarization, common-mode rejection, symmetrical radiation pattern, and seamless integration with differential circuits[1 – 4].

A quasi-Yagi antenna was originally proposed as a single-ended antenna[5] although the driver is differential. Now, the quasi-Yagi antenna is an important type of antennas for end-fire radiation. However, most reported quasi-Yagi antennas are single-ended antennas[5 – 8]. They need to use baluns or complicated feeding networks to convert differential drivers to single-ended inputs, which greatly increases design complexity and degrades antenna performance. In addition, the coupling between two conventional single-ended quasi-Yagi antennas was examined for the design of quasi-Yagi arrays. However, the dominant electromagnetic mechanism and the key structural part for coupling are not clear.

To our best knowledge, the first differential quasi-Yagi antenna[9] was implemented in a thin cavity-down ceramic ball grid array package in low temperature co-fired ceramic (LTCC) technology. It achieved a 10 dB impedance bandwidth of 2.3 GHz from 60.6 GHz to 62.9 GHz and a peak gain of 6 dBi at 62 GHz. The bandwidth was too narrow for 60 GHz radios, which typically require the bandwidth of 7 GHz from 57 GHz to 64 GHz. Furthermore, there has been no differential quasi-Yagi array reported up to now.

In this paper, we present the design, analysis, and measurement of a differential quasi-Yagi antenna and array on high dielectric constant substrates. We design the differential quasi-Yagi antenna and discuss the simulated and measured results in Section 2. We describe the differential quasi-Yagi linear arrays, study the coupling mechanism between the two differential quasi-Yagi antennas, evaluate the effects of decoupling structures, and discuss the simulated and measured results in Section 3. Finally, we draw the conclusion in Section 4.

2 Differential Quasi-Yagi Antenna

Fig. 1 shows the structure and dimensions of the differential quasi-Yagi antenna proposed in this paper. Note that the antenna consists of three elements, namely a driver, a reflector, and a director. The driver is fed by a differential coplanar strip (CPS) line, which is gradually transformed into two single-ended tapered coupled microstrip lines (TCML). More commonly, there are more than one director to improve the antenna gain. The driver and director are horizontally printed on the top surface of a substrate of dielectric constant ε_r, loss tangent δ, length l_s, width w_s, and thickness h. The reflector is

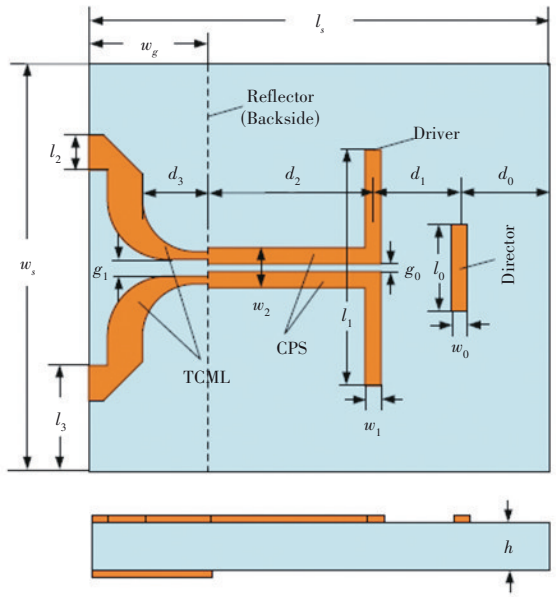

▲Figure 1. Structure and dimensions of the differential quasi-Yagi antenna

usually printed on the bottom surface of the substrate, which has another function as the ground plane.

The design procedure of the differential quasi-Yagi antenna is as follows. It starts with choosing a substrate for the maximum excitation of the surface wave of the TE_0 mode by an electric dipole on the substrate at the central frequency of the operating band. ALEXOPOULOS et al. examined how the substrate affects the excitation of surface waves[10]. They found that the surface wave of the TE_0 mode can be maximumly excited if the critical value of the substrate electrical thickness is satisfied. Using the method described in the classical paper[10], LEONG and ITOH showed that the critical values for the electrical thickness are 0.03, 0.05, and 0.08 for the substrates with ε_r =10.2, 4, and 2.2, respectively[8]. Then, the initial values are set for the length l_0 and width w_0 of the director, the distance d_1 between the director and the driver, the length l_1 and width w_1 of the driver, and the distance d_2 from the driver to the reflector. For simplicity, the same width of $0.02\lambda_0$ can be chosen for the driver and director. The length of the driver is about $0.45\lambda_g$. The length of the director should be shorter than that of the driver and can be $0.3\lambda_g$. The distances between the director and driver and between the driver and reflector are about $0.3\lambda_g$ and $0.25\lambda_g$, respectively. Next, the width w_2 and spacing g_0 of the CPS line can be estimated with the available empirical formula. Finally, the optimum values for the above design parameters can be obtained from High Frequency Structure Simulator (HFSS) simulations.

Fig. 2 shows the photo of the differential quasi-Yagi antenna designed and fabricated on a substrate of dielectric constant ε_r = 10.2 and thickness h=0.635 mm at X-band frequencies. The fabricated dimensions are w_s =15 mm, w_g=4.4 mm,

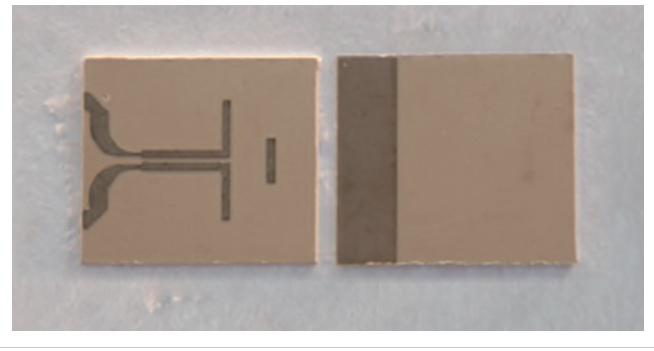

▲Figure 2. Photo of the differential quasi-Yagi antenna

w_0=w_1=0.6 mm, w_2=1.5 mm, l_s=17 mm, l_0=3.2 mm, l_1=8.7 mm, l_2 =1.3 mm, l_3 =3.9 mm, d_0 = 3.3 mm, d_1=3.2 mm, d_2=6.1 mm, g_0=0.3 mm, and g_1=0.6 mm.

Fig. 3 shows the simulated electric field distributions on the top and bottom surfaces of the differential quasi-Yagi antenna. As expected, the surface wave of the TE_0 mode is indeed strongly excited and propagated in the directions normal to the driver. On the one hand, since the polarization direction of the electric field on the driver is the same as that of the electric field on the director, there will be a strong coupling between

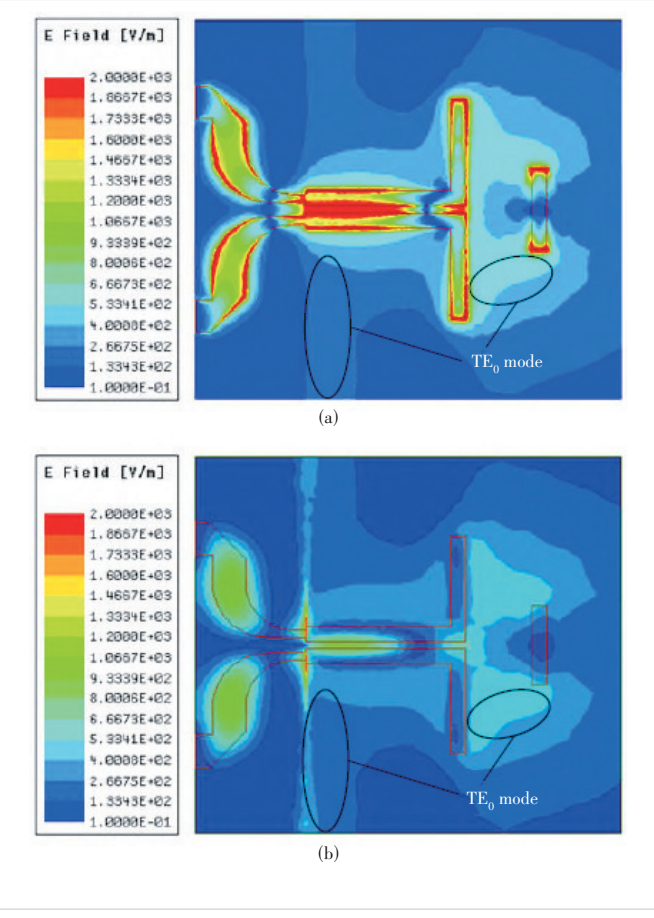

▲Figure 3. Electric field distribution on the (a) top and (b) bottom surfaces

them. Thereby, the surface wave of the TE_0 mode is guided to radiate in the end-fire direction. On the other hand, due to the existence of the ground plane or the reflector, the surface wave of the TE_0 mode cannot be propagated in the grounded substrate region and will be reflected, which further strengthens the radiation in the end-fire direction.

It should be pointed out that the surface wave of the TM_0 mode is quite weakly excited, which can propagate along the axial directions of the driver in both the grounded and ungrounded substrate regions. It causes cross-polarized radiation and deteriorates antenna gain and front-to-back ratio. Therefore, in designing a quasi-Yagi antenna, the major concern is how to excite the surface waves of the TE_0 mode to the greatest extent and the surface waves of the TM_0 mode to the lowest extent.

Fig. 4 shows the simulated and measured $|S_{dd11}|$ of the differential quasi-Yagi antenna as a function of frequency from 7 GHz to 15 GHz. It is evident from the figure that although there are differences between the simulated and measured values, the antenna achieves acceptable matching from 7.5 GHz to 14.8 GHz or a fractional bandwidth of 66% for a voltage standing wave ratio ⩽ 2 at 11.15 GHz. Fig. 5 shows the simulated and measured radiation patterns at 8.2 GHz, 10.6 GHz, and 12.3 GHz. As expected, the antenna radiates an end-fire beam. Fig. 6 shows the simulated and measured gain values. The measured gain values fluctuate between 3.7 dBi and 5.4 dBi from 8 GHz to 12.3 GHz. The simulated radiation efficiency is 94% at 10 GHz. The simulated radiation efficiency at frequencies below 8 GHz and above 13.5 GHz drops quickly, which explains why the gain drops.

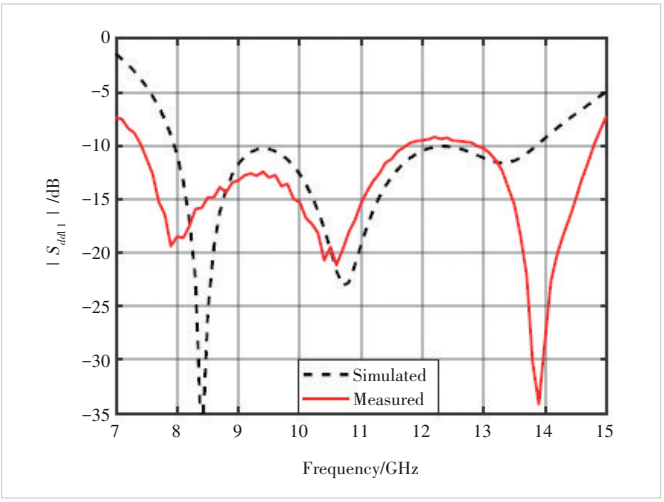

▲ **Figure 4. Simulated and measured $|S_{dd11}|$ of the differential quasi-Yagi antenna**

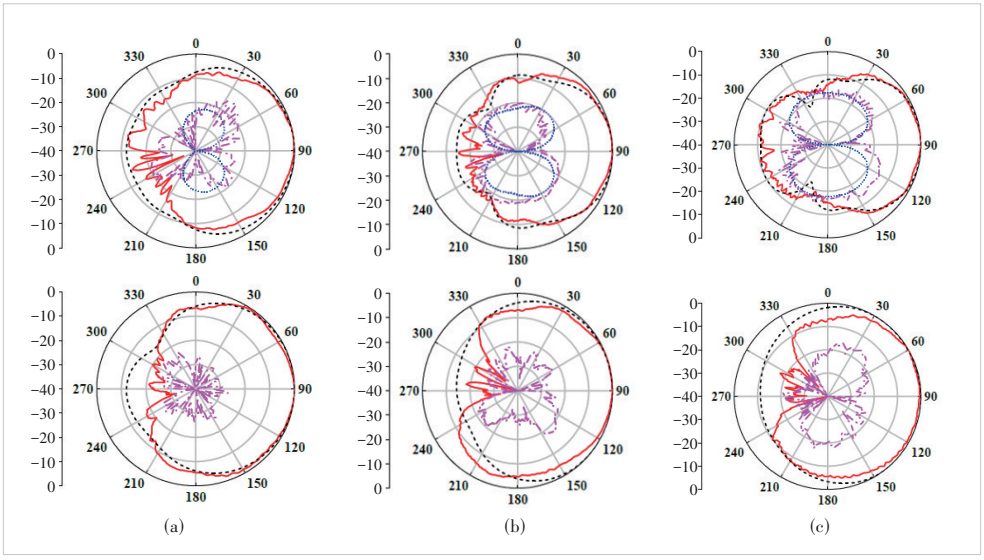

▲ **Figure 5. Simulated and measured E- and H-plane radiation patterns of differential quasi-Yagi antennas at (a) 8.2 GHz, (b) 10.6 GHz, and (c) 12.3 GHz**

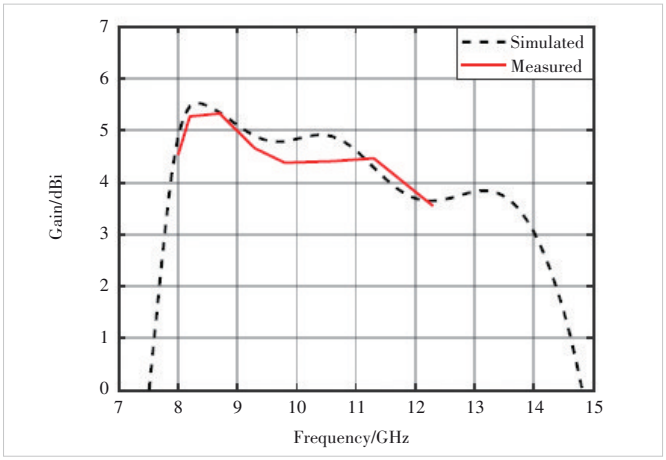

▲ **Figure 6. Simulated and measured gain values of the differential quasi-Yagi antenna**

Table 1 lists the bandwidth, gain, efficiency, cross-polarization (X-pol), and front-to-back ratio (FBR) for the single-ended and differential quasi-Yagi antennas at 10 GHz. It should be mentioned that these quasi-Yagi antennas have the same size and are fabricated with the same material. Note from the table that the differential quasi-Yagi antenna outperforms the single-ended counterparts.

3 Differential Quasi-Yagi Array

The application of the differential quasi-Yagi antenna as an array element is explored in this section. We limit our effort to E-plane linear arrays because we target their potential use in portable and mobile devices[11 – 12].

▼Table 1. Single-ended and differential quasi-Yagi antennas

Reference	Bandwidth/%	Gain/dBi	Efficiency/%	X-pol/dB	FBR/dB
Ref. [7]	48	4.6	93	−12	12
This work	73	4.4	94	−21	15

FBR: front-to-back ratio X-pol: cross-polarization

3.1 Linear Arrays

Fig. 7 shows the top views of the two- and four-element E-plane linear differential quasi-Yagi arrays. The differential quasi-Yagi element is the same as the differential quasi-Yagi antenna presented in the previous section. The distance between the two adjacent elements is d.

3.2 Coupling Mechanism

The mutual coupling between elements needs to be considered especially in the design of a phased array because strong mutual coupling may cause scan blindness. The mutual coupling is determined by the transmission coefficient $|S_{21}|$ or $|S_{dd21}|$ of an array. DEAL et al.[7] determined the E-plane mutual coupling between two single-ended quasi-Yagi antennas implemented on the same substrate to be below − 18 dB and, in most cases, below − 20 dB for the center-to-center spacing equal to or greater than the half wavelength at 10 GHz[7]. They also made an effort to identify the source of mutual coupling and concluded from their measurements of the testing structures that, for a 15-mm-array spacing that corresponds to the half wavelength at the central frequency of 10 GHz, mutual coupling is almost solely due to coupling through the air[7].

To get a deeper insight into the coupling mechanism, we have conducted a simulated study of mutual coupling between two single-ended and two differential quasi-Yagi antennas, respectively. First, we keep the drivers, the substrate, and the truncated ground plane but remove all the other building blocks. Fig. 8(a) shows the simulated electric field distribution on the top surface of the substrate for the case with one driver fed by a lumped port and the other driver matched to a load at

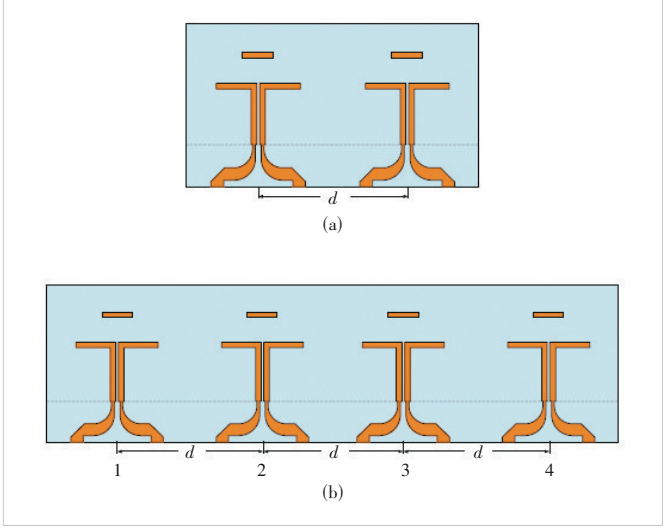

▲Figure 7. Structures of the E-plane linear differential quasi-Yagi arrays of (a) two elements and (b) four elements

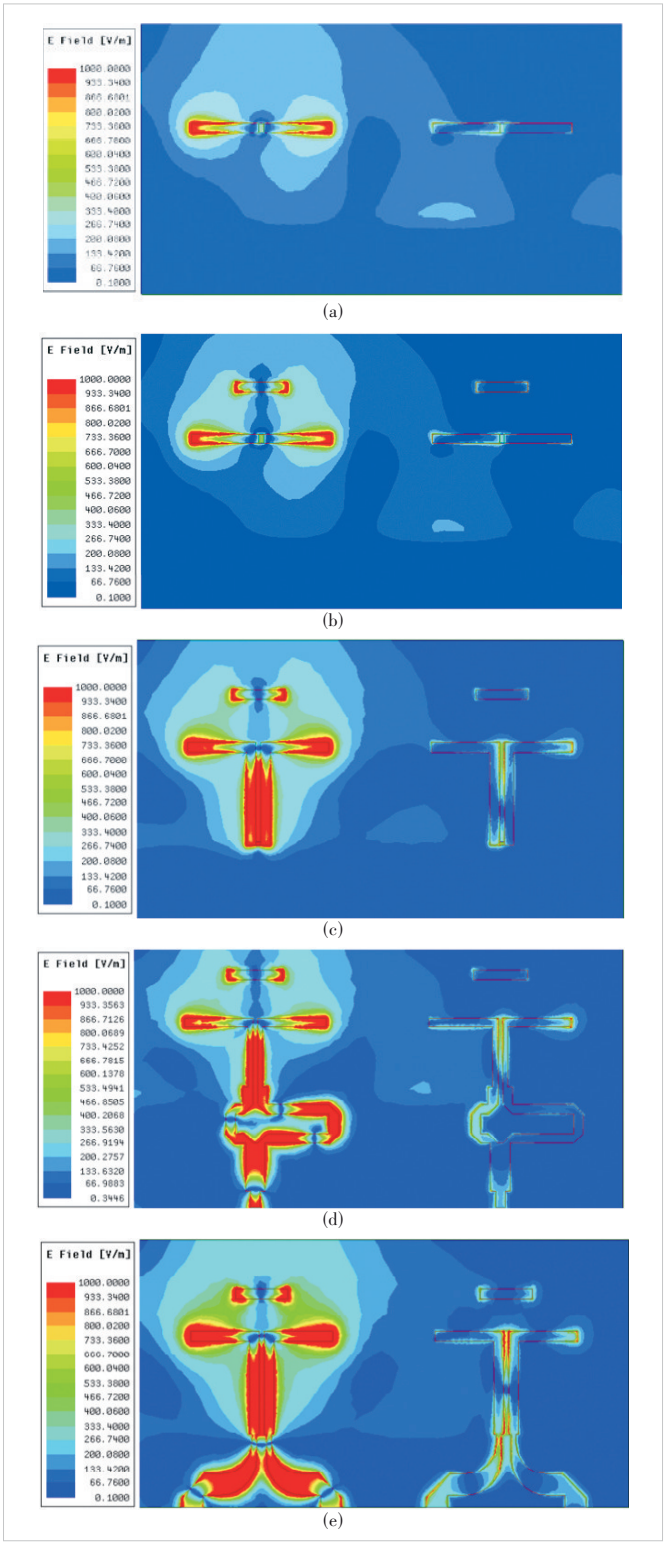

▲Figure 8. Simulated electric field distributions: (a) only driver, (b) driver and director, (c) driver, director and differential coplanar strip (CPS), (d) driver, director, CPS and balun, and (e) driver, director, CPS and tapered coupled microstrip line (TCML)

10 GHz. It is evident from the figure that the surface wave of the TE_0 mode has been strongly excited and trapped in the ungrounded substrate region. It is important to note that the grounded substrate region cuts off the surface wave of the TE_0 mode and forces it to be reflected to the ungrounded substrate region. The reflected surface wave of the TE_0 mode is an important source of mutual coupling. Then, we add two directors in the model, and the simulated electric field distribution on the top surface of the substrate at 10 GHz is shown in Fig. 8 (b). It is seen that there is a strong desirable coupling between the excited driver and its director due to the surface wave of the TE_0 mode for end-fire radiation. There seems no effect by the directors on the coupling between the two drivers. Next, we add CPS lines in the model and move the lumped port to the CPS input and the matched load to the other CPS input. Fig. 8 (c) shows the simulated electric field distribution on the top surface of the substrate at 10 GHz. Note that the CPS lines enhance the coupling between the two drivers. Finally, we add in the model baluns to realize the single-ended quasi-Yagi array and TCML to realize a differential quasi-Yagi array, respectively. Figs. 8(d) and 8(e) show the simulated electric field distributions on the top surfaces of the substrates at 10 GHz for the cases of the single-ended and differential quasi-Yagi arrays, respectively. Note that the coupling is stronger for the differential than for the single-ended quasi-Yagi array.

Fig. 9 shows the simulated $|S_{dd11}|$ and $|S_{dd21}|$ as a function of frequency for the cases in Figs. 8(a) and 8(b) with a spacing of 15 mm between the two elements. As expected, the coupling level over the acceptable matching band from 9 GHz to 11.5 GHz is almost the same between the two cases with and without the directors. Fig. 10 shows the simulated $|S_{dd11}|$ and $|S_{dd21}|$ as a function of frequency for the case in Fig. 8(c) with a spacing of 15 mm between the two elements. Note that the CPS extends the matching band to 15 GHz and reduces the coupling level over a wider bandwidth.

Fig. 11 shows the simulated $|S_{11}|$ and $|S_{21}|$ as a function of frequency for the single-ended quasi-Yagi array of Fig. 8(d) with a spacing of 15 mm between the two elements. Fig. 12 shows the simulated $|S_{dd11}|$ and $|S_{dd21}|$ as a function of fre-

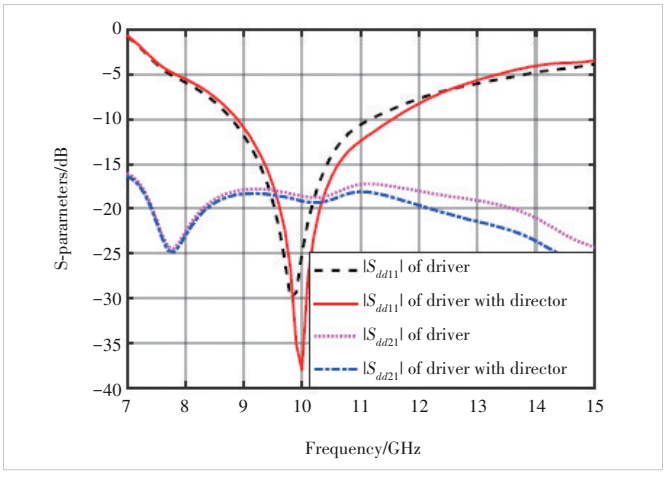

▲ **Figure 9. Simulated $|S_{dd11}|$ and $|S_{dd21}|$ as a function of frequency for the cases in Figs. 8(a) and 8(b)**

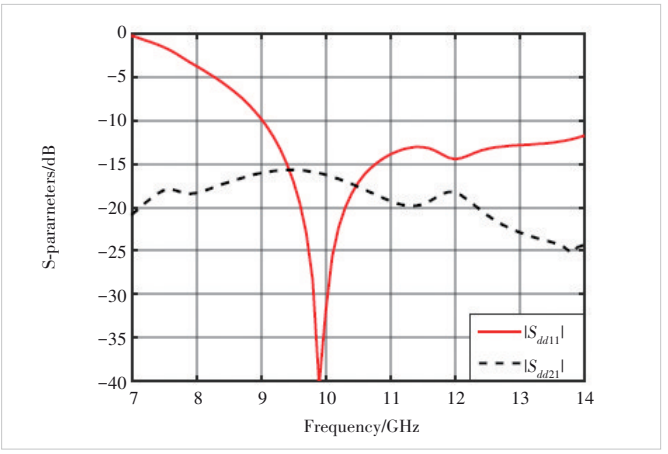

▲ **Figure 10. Simulated $|S_{dd11}|$ and $|S_{dd21}|$ as a function of frequency for the case in Fig. 8(c)**

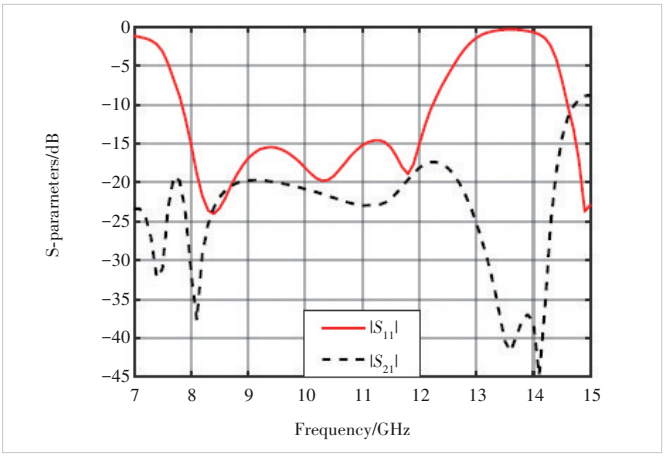

▲ **Figure 11. Simulated $|S_{11}|$ and $|S_{21}|$ as a function of frequency for the single-ended quasi-Yagi array with the spacing of 15 mm between the two elements**

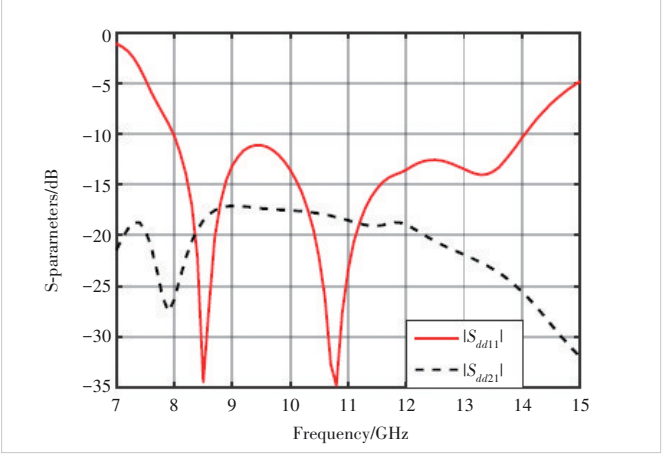

▲ **Figure 12. Simulated $|S_{dd11}|$ and $|S_{dd21}|$ as a function of frequency for the single-ended quasi-Yagi array with a spacing of 15 mm between the two elements**

quency for the differential quasi-Yagi array in Fig. 8(e) with a spacing of 15 mm between the two elements. Note that the matching band is from 7.9 GHz to 12.2 GHz and from 8.0 GHz to 14.0 GHz, respectively, for the single-ended and differential quasi-Yagi arrays. The maximum coupling level is almost the same for the two cases over the respective impedance bandwidths.

3.3 Decoupling Structures and Effects

It is seen from Fig. 12 that the simulated mutual coupling level for the center-to-center spacing of 15 mm, which is equal to the half wavelength at 10 GHz, is – 18 dB. For a multiple-input and multiple-output (MIMO) array, the mutual coupling level of – 25 dB is desirable. Hence, there is a need to further reduce the mutual coupling. A few decoupling structures such as the neutralization line[13], split-ring resonator[14], slit, and air holes have been attempted. The idea to add a meta-surface as a superstrate to reduce the mutual coupling has not been adopted to keep the low profile of the differential quasi-Yagi array[15]. The simulated decoupling effects of the above structures are summarized as follows. For the case of the neutralization line, the coupling level is greatly reduced to −25 dB but the radiation patterns are distorted, and the gain is reduced by 2 dB at 10 GHz. For the case of the split-ring resonator, it fails to reduce the coupling level but increase the gain by 0.2 – 0.7 dB over the impedance bandwidth. For the cases of slit and air holes, they are very effective to reduce the mutual coupling to −25 dB and meanwhile do not affect the impedance bandwidth and radiation patterns. Hence, the E-plane linear arrays with the slit and air holes are fabricated and measured.

3.4 Results and Discussion

Fig. 13 shows the photos of the two-element differential quasi-Yagi arrays without any decoupling structure, with the slit, and with the air holes. The two differential quasi-Yagi antenna elements are separated by 15 mm and fed with the Subminiature version A (SMA)-connected coaxial cables. The slit is a 2 mm wide cut in between the two elements and after the truncated ground plane. The air holes that have the same diameter of 0.5 mm are punched in between the two elements and after the truncated ground plane with an optimized pattern. It should be mentioned that the details of the SMAs and coaxial cables are unknown. The irregular solder joints and curved coaxial cables are hard to be modelled exactly. Hence, only measured results are discussed.

Fig. 14 shows the measured $|S_{dd11}|$ and $|S_{dd21}|$ as a function of frequency for the two-element differential quasi-Yagi arrays without any decoupling structure, with the slit, and with the

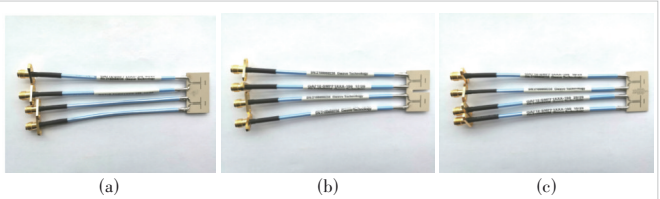

▲ **Figure 13. Photos of the two-element differential quasi-Yagi arrays: (a) solid, (b) slit, and (c) air holes**

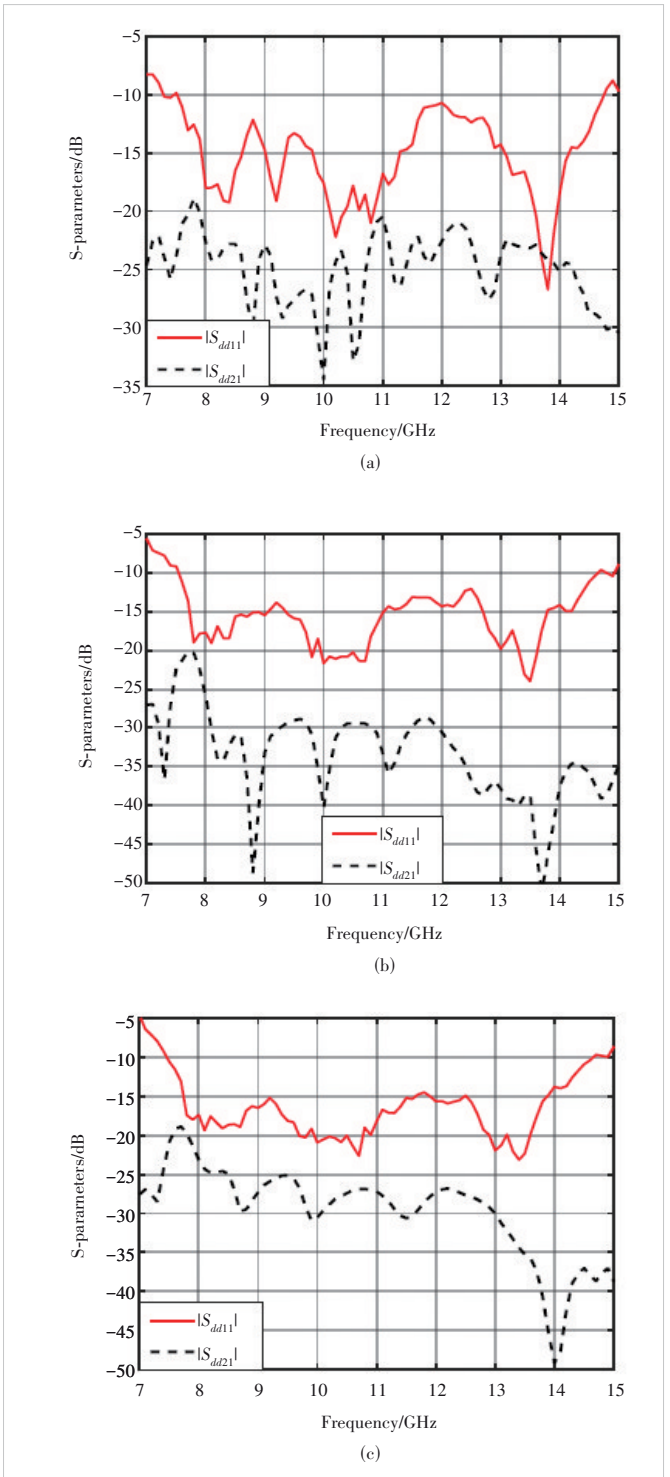

▲ **Figure 14. Measured $|S_{dd11}|$ and $|S_{dd21}|$ as a function of frequency for the differential quasi-Yagi antennas: (a) solid, (b) slit, and (c) air holes**

air holes, respectively. Measured results have confirmed that the simple decoupling structures are quite effective to reduce the mutual coupling level below −25 dB.

Fig. 15 shows the photo of the four-element differential quasi-Yagi array without any decoupling structure. The two adjacent differential quasi-Yagi antenna elements are separated by 0.5 free space wavelength at 10 GHz.

Fig. 16 shows the measured $|S_{dd11}|$ and $|S_{dd21}|$ as a function of frequency for the top two differential quasi-Yagi elements. The measured impedance bandwidth is from 7.6 GHz to 14.3 GHz. The mutual coupling level is below −20 dB over the impedance bandwidth.

Fig. 17 shows the simulated and calculated radiation patterns for the four-element differential quasi-Yagi array at 10 GHz. Due to limitations of our testing facilities, we could not measure the array patterns. We measured the element pattern and obtained the calculated patterns by considering the array factor. It is seen that the calculated and simulated patterns agree quite well for the main lobes. There are differences between the calculated and simulated side lobes.

▲Figure 15. Photo of the four-element differential quasi-Yagi array

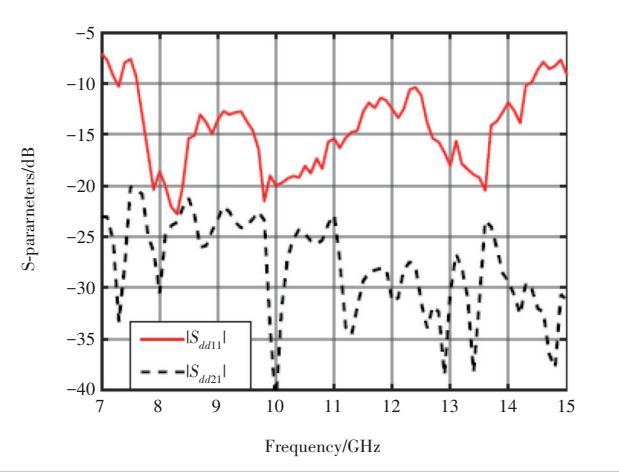

▲Figure 16. Measured $|S_{dd11}|$ *and* $|S_{dd21}|$ as a function of frequency for the four-element differential quasi-Yagi array

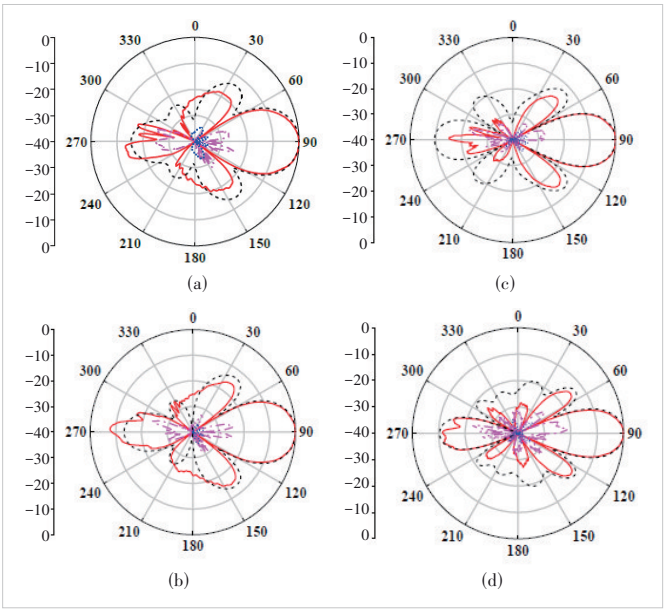

▲Figure 17. Simulated and calculated E-plane radiation patterns of the four-element differential quasi-Yagi array at (a) 8.2 GHz, (b) 8.7 GHz, (c) 10.6 GHz, and (d) 12.3 GHz

4 Conclusions

In this paper, a novel differential quasi-Yagi antenna is presented and compared with a normal single-ended counterpart for the first time. It is found that the differential quasi-Yagi antenna outperforms the conventional single-ended one. The differential quasi-Yagi antenna is then used as an element for E-plane linear arrays. A study of the coupling mechanism between the two differential quasi-Yagi antennas is conducted. The driver is identified to be the decisive part for the mutual coupling. Four decoupling structures and their effects are evaluated. The arrays with simple but effective decoupling structures are fabricated and measured. The measured results demonstrate that the coupling levels of these arrays can be reduced to less than − 25 dB over the broad bandwidth and the simple slit or air-hole decoupling structure has a negligible effect on the impedance matching and radiation patterns of the arrays. It is anticipated that the differential quasi-Yagi antenna, as a promising antenna candidate, should find wide applications in wireless communication systems, power combining, phased, active, imaging, and MIMO arrays.

References

[1] ZHANG Y P, WANG J J, LI Q, et al. Antenna-in-package and transmit-receive switch for single-chip radio transceivers of differential architecture [J]. IEEE transactions on circuits and systems I: regular papers, 2008, 55(11): 3564 − 3570. DOI: 10.1109/TCSI.2008.925822

[2] ZHANG Y P, WANG J J. Theory and analysis of differentially-driven microstrip antennas [J]. IEEE transactions on antennas and propagation, 2006, 54(4): 1092 − 1099. DOI: 10.1109/TAP.2006.872597

[3] ZHANG Y P. Design and experiment on differentially-driven microstrip anten-

nas [J]. IEEE transactions on antennas and propagation, 2007, 55(10): 2701 – 2708. DOI: 10.1109/TAP.2007.905832
[4] WHITE C R, REBEIZ G M. A differential dual-polarized cavity-backed microstrip patch antenna with independent frequency tuning [J]. IEEE transactions on antennas and propagation, 2010, 58(11): 3490 – 3498. DOI: 10.1109/TAP.2010.2071364
[5] QIAN Y, DEAL W R, KANEDA N, et al. Microstrip-fed quasi-yagi antenna with broadband characteristics [J]. Electronics letters, 1998, 34(23): 2194. DOI: 10.1049/el: 19981583
[6] SOR J, QIAN Y X, ITOH T. Coplanar waveguide fed quasi-Yagi antenna [J]. Electronics letters, 2000, 36(1): 1. DOI: 10.1049/el: 20000132
[7] DEAL W R, KANEDA N, SOR J, et al. A new quasi-yagi antenna for planar active antenna arrays [J]. IEEE transactions on microwave theory and techniques, 2000, 48(6): 910 – 918. DOI: 10.1109/22.846717
[8] LEONG K M K H, ITOH T. Printed quasi-yagi antennas [M]//Printed Antennas for Wireless Communications. Chichester, UK: John Wiley & Sons, Ltd, 2007: 69 – 102. DOI: 10.1002/9780470512241.ch3
[9] SUN M, ZHANG Y P, CHUA K M, et al. Integration of yagi antenna in LTCC package for differential 60-GHz radio [J]. IEEE transactions on antennas and propagation, 2008, 56(8): 2780 – 2783. DOI: 10.1109/tap.2008.927577
[10] ALEXOPOULOS N G, KATEHI P B, RUTLEDGE D B. Substrate optimization for integrated circuit antennas [J]. IEEE transactions on microwave theory and techniques, 1983, 31(7): 550 – 557. DOI: 10.1109/TMTT.1983.1131544
[11] GU X X, LIU D X, BAKS C, et al. A multilayer organic package with four integrated 60GHz antennas enabling broadside and end-fire radiation for portable communication devices [C]//65th Electronic Components and Technology Conference (ECTC). IEEE, 2015: 1005 – 1009. DOI: 10.1109/ECTC.2015.7159718
[12] KIM H T, PARK B S, SONG S S, et al. A 28-GHz CMOS direct conversion transceiver with packaged 2 × 4 antenna array for 5G cellular system [J]. IEEE journal of solid-state circuits, 2018, 53(5): 1245 – 1259. DOI: 10.1109/JSSC.2018.2817606
[13] DIALLO A, LUXEY C, LE THUC P, et al. Study and reduction of the mutual coupling between two mobile phone PIFAs operating in the DCS1800 and UMTS bands [J]. IEEE transactions on antennas and propagation, 2006, 54 (11): 3063 – 3074. DOI: 10.1109/TAP.2006.883981
[14] BAIT-SUWAILAM M M, SIDDIQUI O F, RAMAHI O M. Mutual coupling reduction between microstrip patch antennas using slotted-complementary split-ring resonators [J]. IEEE antennas and wireless propagation letters, 2010, 9: 876 – 878. DOI: 10.1109/LAWP.2010.2074175
[15] SÁENZ E, EDERRA I, GONZALO R, et al. Coupling reduction between dipole antenna elements by using a planar meta-surface [J]. IEEE transactions on antennas and propagation, 2009, 57(2): 383 – 394. DOI: 10.1109/TAP.2008.2011249

Biographies

ZHU Zhihao received his BS degree from Hangzhou Dianzi University, China in 2016. He is currently pursuing an MS degree in electronic science and technology with Shanghai Jiao Tong University, China. His research interests include antenna theory and design, especially in shorted patch antennas, broadband printed antennas, antenna decoupling, and antenna-in-package (AiP).

ZHANG Yueping (eypzhang@ntu.edu.sg) is a full professor with the School of Electrical and Electronic Engineering, Nanyang Technological University, Singapore. He is a Distinguished Lecturer of the IEEE Antennas and Propagation Society (IEEE AP-S) and Fellow of the IEEE. He was a member of the IEEE AP-S Field Award Committee (2015 – 2017) and an associate editor of *IEEE Transactions on Antennas and Propagation* (2010 – 2016). Prof. ZHANG has published numerous papers, including two invited papers and one regular paper in the *Proceedings of the IEEE* and one invited paper in *IEEE Transactions on Antennas and Propagation*. He is a Chinese radio scientist who has published a historical article in English learned journals such as the *IEEE Antennas and Propagation Magazine*. He received the 2012 IEEE AP-S Sergei A. Schelkunoff Prize Paper Award. Prof. ZHANG has been invited to deliver plenary speeches at the flagship conferences organized by IEEE, CIE, EurAAP, and IEICE. He received the Best Paper Award from the 2nd IEEE/IET International Symposium on Communication Systems, Networks and Digital Signal Processing, the Best Paper Prize from the 3rd IEEE International Workshop on Antenna Technology, and the Best Paper Award from the 10th IEEE Global Symposium on Millimeter-Waves. He holds seven US patents. He has made pioneering and significant contributions to the development of AiP technology. He received the 2020 IEEE AP-S John Kraus Antenna Award. His current interests are in the development of antenna-on-chip (AoC) technology for very large-scale antenna integration and characterization of chip-scale propagation channels at terahertz for wireless chip area networks (WCAN).